Study on the Influence of Channel's Non-Ideal Characteristic on Pseudo-Code Measurement Bias for GNSS Receiver

Yaoding WANG, Xiang FAN, Mimi LU

Beijing Institute of Tracking and Telecommunication Technology, Beijing, 100094, China

wangyaodingsdu@126.com, 13810338459@163.com, mimiucatherine@163.com

Submitted December 9, 2025 / Accepted March 22, 2026 / Online first April 20, 2026

Abstract. *GNSS has been widely used in civilian and military areas due to its high precision. However, the channel's non-ideal characteristic may introduce pseudo-code measurement bias to degrade positioning precision. There are few theoretical analyses for interpreting why the channel's non-ideal characteristic may introduce pseudo-code measurement bias and what kind of channels will not introduce pseudo-code measurement bias. We have conducted a systematical study on the above issues. Firstly, we established an analysis model for interpreting the channel' non-ideal characteristic's influence on pseudo-code measurement bias. Based on the analysis model, we proposed four sufficient conditions for unbiased pseudo-code measurement. Secondly, we applied the analysis model to typical channels, i.e. sine type group delay channel, frequency-domain anti-jamming channel and space-domain anti-jamming channel, to evaluate the channel's influence on pseudo-code measurement bias. Finally, we conducted simulations to evaluate the theoretical analysis' correctness. Results show that these typical channels do not introduce pseudo-code measurement bias, which are consistent with theoretical analysis. As a result, the correctness of the proposed four sufficient conditions is verified so that the proposed four sufficient conditions can be used to guide the design of unbiased pseudo-code measurement channel.*

Keywords

Channel characteristic, pseudo-code measurement bias, GNSS receiver, non-ideal

1. Introduction

GNSS has been applied in many civilian and military areas due to its high precision, all day and all weather. Pseudo-code measurement is one of the most important measurements for GNSS receiver positioning. There are several factors that can introduce pseudo-code measurement bias, i.e. satellite clock bias, satellite orbit bias, tropospheric delay, ionospheric delay, multipath and channel's non-ideal characteristic [1]. In addition, if GNSS receiver uses antenna array to mitigate jam, antenna array anti-jamming algorithms can also introduce pseudo-code measurement bias [2]. Pseudo-code measurement biases introduced by satellite clock bias, satellite orbit bias, tropospheric delay and ionospheric delay can be mitigated by empirical models [3–5]. Pseudo-code measurement bias introduced by multipath can be mitigated by anti-multipath algorithms [6], [7]. Pseudo-code measurement bias introduced by the antenna array anti-jamming algorithms can be mitigated by some special constraints for antenna element weights [8–10]. After the above processing, most of pseudo-code measurement biases can be mitigated. In this case, channel's non-ideal characteristic becomes the main factor introducing pseudo-code measurement bias.

If channel characteristic is ideal, it will introduce a static delay depending on the channel. This static delay can be measured and corrected in advance so that it will not degrade positioning. However, due to device errors, the channel cannot be completely ideal. Many researchers concerned on channel's non-ideal characteristic and did some beneficial research works. These researches can be divided into two categories, i.e. researches about channel's non-ideal characteristic itself and researches about the influence of channel's non-ideal characteristic on pseudo-code measurement. For researches about channel's non-ideal characteristic itself, Zhu X. W. et al. proposed a decomposition model of group delay based on Taylor series to analyze channel's non-ideal characteristic [11]; Xiao Z. B. et al. pointed out that Zhu X. W. et al.'s model could not be applied to channel's non-ideal characteristic with trigonometric features so that they proposed a Fourier decomposition model of group delay based on trigonometric function series [12]; Zhu X. W. et al. and Xiao Z. B. et al. both did good work for analyzing channel's non-ideal characteristic. For researches about the influence of channel's non-ideal characteristic on pseudo-code measurement, many researchers did good researches from different point. Liu Y. Q. et al. analyzed the relationship between pseudo-code measurement bias and the group delay of channel. They implemented Taylor transformation on group delay and found that the second-order group delay

DOI: 10.13164/re.2026.0208

played an important role in introducing pseudo-code measurement bias [13]. However, they mainly concerned phase frequency response of channel's non-ideal characteristic and did not study the amplitude frequency response of channel's non-ideal characteristic. Zhou H. W. et al. analyzed the pseudo-code measurement bias introduced by the satellite payload's non-ideal characteristic [14]. Betz J. W. analyzed the GNSS signal' characteristic after it passed the non-ideal channel [15]. Soellner M. et al. proposed several models of the channel's non-ideal characteristic and analyzed their influence on the distortion of the GNSS signal [16]. Both Betz J. W. and Soellner M. et al. analyzed several different channels' non-ideal characteristics' influence on pseudo-code measurement biases. Hauschild A. et al. analyzed the influence of correlator's spacing on pseudo-code measurement bias when channel's characteristic is non-ideal and pointed out that the difference of pseudo-code measurement biases between different correlators' spacing could reach to several meters [17]. They also analyzed the difference of pseudo-code measurement biases introduced by channel's non-ideal characteristic between different satellites [18]. Muller T. analyzed the influence of channel characteristic on pseudo-code measurement bias when channel characteristic was SAW-filter [19]. Zhang T Q et al. analyzed the influence of channel characteristic on pseudo-code measurement bias when channel characteristic was frequency domain anti-jamming filter [20]. Unlike others researches, Zhang T. Q. et al. studied the influence of the amplitude frequency response of channel's non-ideal characteristic on pseudo-code measurement bias.

In a whole, above researches are in depth and comprehensive, but they did not answer the following two questions. Firstly, why the channel's non-ideal characteristic may introduce pseudo-code measurement bias? Secondly, will channel's non-ideal characteristic necessarily introduce pseudo-code measurement bias? In other words, what kind of channels will not introduce pseudo-code measurement bias? In this paper, we will answer these two questions systemically. The main contributions of the paper are as follows. Firstly, we proposed an analysis model for analyzing the influence of channel's non-ideal characteristic on pseudo-code measurement bias. This analysis model includes both amplitude and phase frequency response of channel characteristic. Secondly, we proposed four sufficient conditions of channel's non-ideal characteristic for un-biased pseudo-code measurement. Thirdly, we applied the proposed analysis model to typical channels and analyzed the influence of these typical channels on pseudo-code measurement bias. Simulations verify the correctness of the proposed sufficient conditions. As a result, the proposed sufficient conditions can be used to guide the channel design for unbiased pseudo-code measurement.

The analysis model and four sufficient conditions for unbiased pseudo-code measurement are introduced in the following part. Then, we applied the analysis model to typical channels. Next, a large number of simulations are conducted to evaluate theoretical analysis' correctness. Finally, conclusions are drawn.

2. Analysis Model

The GNSS signal can be expressed as follows [1]:

$$s_{\mathrm{i}}(t) = Ac(t-\tau_i)\mathrm{e}^{\mathrm{j}2\pi f_{\mathrm{i}}t+\mathrm{j}\phi_{\mathrm{i}}} \tag{1}$$

where $c(t)$ is pseudo-code signal which is a real function, A, τ_{i}, f_{i}, and Φ_{i} are magnitude, delay, frequency and carrier phase of the GNSS signal, respectively. The GNSS signal passes through the radio frequency channel, and then the GNSS receiver generates estimated pseudo-code and carrier phase locally to demodulate and dispread the GNSS signal and the outcome is used for pseudo-code measuring. Defining the radio frequency channel time-domain function and frequency-domain function as $h(t)$ and $H(f)$, respectively, the GNSS signal after passing through the radio frequency channel can be expressed as follows:

$$s_{\mathrm{o}}(t) = s_{\mathrm{i}}(t) * h(t) \tag{2}$$

where $*$ is the convolution operator. Generally, the GNSS signal and the radio frequency channel are linear time-invariant and can be implemented Fourier transform [11], [12]. The estimated pseudo-code and carrier phase can be expressed as $c(t-\hat{\tau_{\mathrm{i}}})$ and $\exp(-\mathrm{j}2\pi\hat{f_{\mathrm{i}}}t - \mathrm{j}\Phi_{\mathrm{o}})$, respectively, where $\hat{\tau_{\mathrm{i}}}$, $\hat{f_{\mathrm{i}}}$ and Φ_{o} are the estimated delay, the estimated frequency and the local carrier phase, respectively. The outcome after demodulated and dispread can be expressed as follows [1]:

$$\begin{aligned} r_{\mathrm{o}}\left(\hat{\tau}_{\mathrm{i}}, \hat{f}_{\mathrm{i}}\right) &= \int_{-\infty}^{+\infty} r_{\mathrm{c}}\left(\hat{\tau}_{\mathrm{i}} - \tau_{\mathrm{i}} - p\right) h(p)\mathrm{e}^{-\mathrm{j}2\pi f_{\mathrm{i}}p}\,\mathrm{d}p \\ &\cdot \mathrm{sinc}\left(f_{\mathrm{e}}T_{\mathrm{coh}}\right)\mathrm{e}^{\mathrm{j}2\pi f_{\mathrm{e}}\left(t_1+\frac{T_{\mathrm{coh}}}{2}\right)} \cdot \mathrm{e}^{-\mathrm{j}\phi_{\mathrm{e}}} \end{aligned} \tag{3}$$

where f_{e} is the difference between the GNSS signal frequency and the estimated frequency, Φ_{e} is the difference between the GNSS signal carrier phase and the local carrier phase, $\mathrm{sinc}(\cdot)$ is the sinc function, T_{coh} is the integration time, t_1 is the initial integration time, $r_{\mathrm{c}}(\tau)$ is the auto-correlate function of pseudo-code signal. $r_{\mathrm{c}}(\tau)$ can be calculated as follows:

$$r_{\mathrm{c}}(\tau) = \int_{-\infty}^{+\infty} c(t)c(t-\tau)\,\mathrm{d}t. \tag{4}$$

As formula (4) shows, $r_{\mathrm{c}}(\tau)$ is symmetric and a real even function. Figure 1 shows the GNSS signal processing flow chart.

Defining function $g(t)$ as follows:

$$g(t) = h(t)\mathrm{e}^{-\mathrm{j}2\pi f_{\mathrm{i}}t}. \tag{5}$$

Obviously, $g(t)$ is the baseband form of the $h(t)$. Substituting formula (5) into (3), we can get the following formula:

$$\begin{aligned} &r_{\mathrm{o}}\left(\hat{\tau}_{\mathrm{i}}, \hat{f}_{\mathrm{i}}\right) = \\ &r_{\mathrm{c}}\left(\hat{\tau}_{\mathrm{i}} - \tau_{\mathrm{i}}\right) * g\left(\hat{\tau}_{\mathrm{i}}\right)\mathrm{sinc}\left(f_{\mathrm{e}}T_{\mathrm{coh}}\right)\mathrm{e}^{\mathrm{j}2\pi f_{\mathrm{e}}\left(t_1+\frac{T_{\mathrm{coh}}}{2}\right)}\mathrm{e}^{-\mathrm{j}\phi_{\mathrm{e}}}. \end{aligned} \tag{6}$$

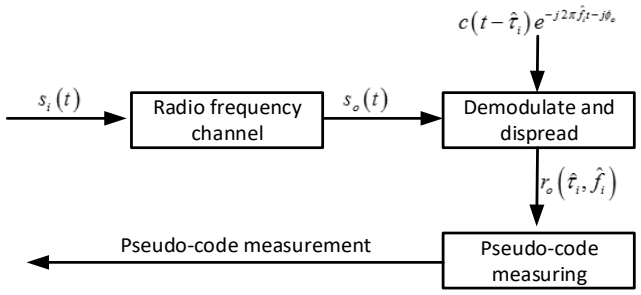

Fig. 1. GNSS signal processing flow chart.

When the tracking loop is running stably, f_e tends to zero. Then, formula (6) can be simplified as follows:

$$r_o(\hat{\tau}_i) = r_c(\hat{\tau}_i - \tau_i) * g(\hat{\tau}_i) \cdot e^{-j\phi_e}. \quad (7)$$

For the GNSS receiver, it usually uses incoherent integration discriminator for pseudo-code measuring. The incoherent integration can be calculated as follows:

$$\left|r_o(\hat{\tau}_i)\right| = \left|r_c(\hat{\tau}_i - \tau_i) * g(\hat{\tau}_i)\right| \quad (8)$$

where $|\cdot|$ is modulo operation. The discriminator function can be calculated as follows [1]:

$$\zeta_{code} = \frac{1}{2}\frac{\left|r_o\left(\hat{\tau}_i - \frac{d}{2}\right)\right| - \left|r_o\left(\hat{\tau}_i + \frac{d}{2}\right)\right|}{\left|r_o\left(\hat{\tau}_i - \frac{d}{2}\right)\right| + \left|r_o\left(\hat{\tau}_i + \frac{d}{2}\right)\right|} \quad (9)$$

where d is the interval of the early code and the late code. As formula (9) shows, when $|r_c(\tau_i)|$ is symmetric, there will be no pseudo-code measurement bias. As formula (8) shows, although $|r_c(\hat{\tau_i} - \tau_i)|$ is symmetric, when it is convoluted with $g(\hat{\tau_i})$ which is determined by the channel, the outcome may be asymmetric so that pseudo-code measurement bias is introduced. This is the reason why channel's non-ideal characteristic may introduce pseudo-code measurement bias.

Defining function $r(\tau)$ as follows:

$$r(\tau) = r_c(\tau - \tau_i) * g(\tau). \quad (10)$$

Assuming that $r(\tau)$ is symmetric about $\tau = \tau_i'$, where τ_i' is the GNSS signal's delay after it passes through the channel, we can get the following formula:

$$\left|r(\tau_i' + \tau)\right| = \left|r(\tau_i' - \tau)\right|. \quad (11)$$

Based on (11), we propose four sufficient conditions of channel characteristic for unbiased pseudo-code measurement.

Condition 1:

$$r(\tau_i' + \tau) = r(\tau_i' - \tau) \quad (12)$$

Implementing Fourier transform on both sides of (12), we can get the following formula:

$$e^{j2\pi f\tau_i'} R(f) = e^{-j2\pi f\tau_i'} R(-f) \quad (13)$$

where $R(f)$ is the Fourier transform of $r(\tau)$. Implementing Fourier transform on both sides of (10), $R(f)$ can be calculated as follows:

$$R(f) = e^{-j2\pi f\tau_i} R_c(f) G(f) \quad (14)$$

where $R_c(f)$ and $G(f)$ are the Fourier transforms of $r_c(\tau)$ and $g(\tau)$. Because $r_c(\tau)$ is an even function, $R_c(\tau)$ is a real even function. Implementing Fourier transform on both sides of (5), $G(f)$ can be calculated as follows:

$$G(f) = H(f + f_i). \quad (15)$$

Obviously, $G(f)$ is the baseband form of $H(f)$. Substituting formula (14) and (15) into (13), we can get the following formula:

$$\begin{aligned} &e^{j2\pi f(\tau_i' - \tau_i)} R_c(f) H(f + f_i) \\ &= e^{-j2\pi f(\tau_i' - \tau_i)} R_c(-f) H(-f + f_i) e^{j\theta}. \end{aligned} \quad (16)$$

As mentioned earlier, τ_i is the GNSS signal's delay before it passes through the channel and τ_i' is the GNSS signal's delay after it passes through the channel. As a result, $\tau_i' - \tau_i$ is the delay introduced by the channel. Defining function as follows:

$$Q(f) = e^{j2\pi f(\tau_i' - \tau_i)} H(f + f_i). \quad (17)$$

Let's discuss the physical interpretation of $Q(f)$. At first, $H(f + f_i)$ is the baseband form of the channel; then, $\tau_i' - \tau_i$ is the delay introduced by the channel so that $\exp[j2\pi f(\tau_i' - \tau_i)]$ is the compensation of delay introduced by the channel. As a result, $Q(f)$ is the baseband channel response after channel delay compensation. Substituting formula (17) into (16) and considering that $R_c(f)$ is a real even function, we can get the following judgment formula:

$$Q(f) = Q(-f). \quad (18)$$

As formula (18) shows, $Q(f)$ is an even function in this case. Let's discuss the reason why this feature of $Q(f)$ will not introduce pseudo-code measurement bias. Substituting formula (5) into (10), we can find that formula (10) is equal to the convolution of $r_c(\tau)$ and the time-domain function of $Q(f)$. Because formula (18) holds true, the time-domain function of $Q(f)$ is even symmetric. As formula (4) shows, $r_c(\tau)$ is even symmetric, too. As a result, $r(\tau)$ is symmetric in this case so that no pseudo-code measurement bias will be introduced.

In practice, given the channel characteristic's frequency-domain function $H(f)$, we can get $Q(f)$ by formula (17); then, we can judge whether formula (18) holds true and if formula (18) holds true, formula (16) holds true, as a result, formula (13) holds true so that formula (12) holds true which means condition 1 holds true so that no pseudo-code measurement bias will be introduced.

Condition 2:

$$r\left(\tau_{\mathrm{i}}'+\tau\right)=-r\left(\tau_{\mathrm{i}}'-\tau\right) \tag{19}$$

The derivation process of condition 2 is similar to condition 1 and the judgment formula is as follows:

$$Q(f)=-Q(-f). \tag{20}$$

As formula (20) shows, $Q(f)$ is an odd function. In this case, the time-domain function of $Q(f)$ is odd symmetric. Similar to condition 1, $r(\tau)$ is symmetric in this case so that no pseudo-code measurement bias will be introduced.

Condition 3:

$$r\left(\tau_{\mathrm{i}}'+\tau\right)=r^{*}\left(\tau_{\mathrm{i}}'-\tau\right) \tag{21}$$

where $(\cdot)^{*}$ is conjugate operation. The derivation process of condition 3 is similar to condition 1 and the judgment formula is as follows:

$$Q(f)=Q^{*}(f). \tag{22}$$

As formula (22) shows, $Q(f)$ is a real function. In this case, the time-domain function of $Q(f)$ is conjugate symmetric. Similar to condition 1, $r(\tau)$ is symmetric in this case so that no pseudo-code measurement bias will be introduced.

Condition 4:

$$r\left(\tau_{\mathrm{i}}'+\tau\right)=-r^{*}\left(\tau_{\mathrm{i}}'-\tau\right) \tag{23}$$

The derivation process of condition 4 is similar to condition 1 and the judgment formula is as follows:

$$Q(f)=-Q^{*}(f). \tag{24}$$

As formula (24) shows, $Q(f)$ is an imaginary function in this case. In this case, the time-domain function of $Q(f)$ is conjugate anti-symmetric. Similar to condition 1, $r(\tau)$ is symmetric in this case so that no pseudo-code measurement bias will be introduced

Table 1 summarizes these four sufficient conditions of channel characteristic for unbiased pseudo-code measurement.

One point should be pointed out is that these four conditions are sufficient conditions for unbiased pseudo-code measurement, but they are not necessary conditions. The reason is that if formula (12) or (19) or (21) or (23) holds true, we can deduce that formula (11) holds true. However, if formula (11) holds true, we cannot deduce that

Number	Sufficient condition
1	$Q(f)$ is an even function
2	$Q(f)$ is an odd function
3	$Q(f)$ is a real function
4	$Q(f)$ is an imaginary function

Tab. 1. Four sufficient conditions of channel characteristic for unbiased pseudo-code measurement.

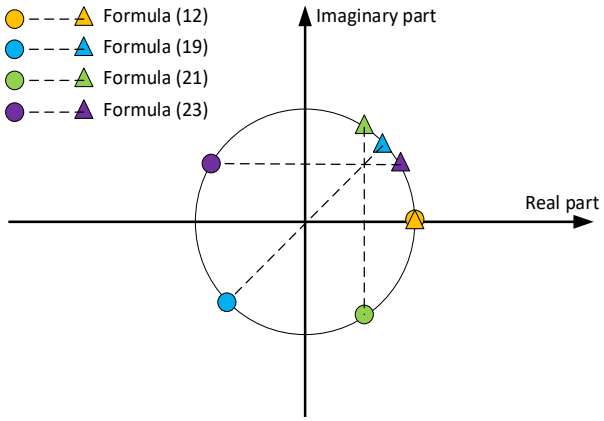

Fig. 2. Schematic diagram when the modules of two complex numbers are equal.

formula (12) or (19) or (21) or (23) holds true. Figure 2 shows the schematic diagram when the modules of two complex numbers are equal. The X-axis and Y-axis represent the real part and the imaginary part of a complex number, respectively. Circle and triangle represent two complex numbers. If the modules of two complex numbers are equal, these two complex numbers are on the same circle. As Figure 2 shows, formula (12) (shown in yellow), (19) (shown in blue), (21) (shown in green) and (23) (shown in purple) are four exceptional cases where the modules of two complex numbers are equal. In practice, as long as one of these four conditions holds true, there will be no pseudo-code measurement bias. This conclusion can guide channel design for unbiased pseudo-code measurement. In fact, reference [10] applied condition 1 in designing array antenna weights to achieve unbiased pseudo-code measurement. However, because these four conditions are not necessary conditions, we cannot confirm that there will definitely be pseudo-code measurement bias when these four conditions do not hold true. In other words, these four conditions can guide channel design for unbiased pseudo-code measurement, but they are not the criterion for determining whether a channel will introduce pseudo-code measurement bias.

3. Analysis on Typical Channels

Channel frequency-domain function $H(f)$ can be expressed as follows [12]:

$$H(f)=\left|H(f)\right|\mathrm{e}^{\mathrm{j}\arg\left(H(f)\right)} \tag{25}$$

where $|H(f)|$ and $\arg(H(f))$ are amplitude frequency response and phase frequency response of the channel, respectively. Group delay is an important parameter of channel and it can be calculated as follows [12]:

$$\gamma(f)=-\frac{1}{2\pi}\frac{\mathrm{d}\left[\arg\left(H(f)\right)\right]}{\mathrm{d}f}. \tag{26}$$

We can use group delay to describe the phase frequency response of the channel.

3.1 Sine Type Group Delay Channel

The group delay of radio frequency channel can be expressed as follows [12]:

$$\gamma_{\sin}(f) = \alpha \sin\left(2\pi \frac{(f - f_{\mathrm{i}})}{\beta}\right) \tag{27}$$

where α and β are magnitude coefficient and frequency coefficient of the sine type group delay. The phase frequency response can be calculated as follows [12]:

$$\arg\left(H_{\sin}(f)\right) = \alpha\beta \cos\left(2\pi \frac{(f - f_{\mathrm{i}})}{\beta}\right). \tag{28}$$

Set the amplitude frequency response as 1, the channel frequency-domain function can be calculated as follows:

$$H_{\sin}(f) = \mathrm{e}^{\mathrm{j}\left(\alpha\beta\cos\left(2\pi\frac{(f-f_{\mathrm{i}})}{\beta}\right)\right)}. \tag{29}$$

Substituting formula (29) into (17), we can find $Q(f)$ is an even function which means that condition 1 holds true. As a result, sine type group delay channel will not introduce pseudo-code measurement bias.

3.2 Frequency-Domain Anti-Jamming Channel

The amplitude frequency response of radio frequency channel can be expressed as follows [20]:

$$\left|H_{\text{Fre-anti-jam}}(f)\right| = \begin{cases} 0, & f_{\mathrm{i}} + f_{\mathrm{J}} - \dfrac{f_{\mathrm{B}}}{2} \le f \le f_{\mathrm{i}} + f_{\mathrm{J}} + \dfrac{f_{\mathrm{B}}}{2} \\ 1, & \text{others} \end{cases} \tag{30}$$

where f_{J} is the offset of the jamming center frequency relative to the GNSS signal frequency and f_{B} is the jamming bandwidth. Assuming that the phase frequency response is linear and the group delay is t_0, the phase frequency response can be calculated as follows [20]:

$$\arg\left(H_{\text{Fre-anti-jam}}(f)\right) = -2\pi(f - f_{\mathrm{i}})t_0. \tag{31}$$

The channel frequency-domain function can be calculated as follows:

$$H_{\text{Fre-anti-jam}}(f) = \begin{cases} 0, & f_{\mathrm{i}} + f_{\mathrm{J}} - \dfrac{f_{\mathrm{B}}}{2} \le f \le f_{\mathrm{i}} + f_{\mathrm{J}} + \dfrac{f_{\mathrm{B}}}{2} \\ \mathrm{e}^{\mathrm{j}(-2\pi(f-f_{\mathrm{i}})t_0)}, & \text{others} \end{cases} \tag{32}$$

Substituting formula (32) into (17), we can find $Q(f)$ is a real function which means that condition 3 holds true. As a result, frequency-domain anti-jamming channel will not introduce pseudo-code measurement bias.

3.3 Space-Domain Anti-Jamming Channel

The channel frequency-domain function can be expressed as follows [21]:

$$H_{\text{Spa-anti-jam}}(f) = \mathbf{w}^{\mathrm{H}}\mathbf{v}_{\mathrm{s}} \tag{33}$$

where $\mathbf{w} = (w_1\, w_2 \ldots w_N)^{\mathrm{T}}$ is the $N \times 1$ dimensional antenna array weight vector, N is the number of antenna elements, w_n is the weight of the n-th antenna element, $(\cdot)^{\mathrm{H}}$ denotes the conjugate transpose, and $(\cdot)^{\mathrm{T}}$ denotes the transpose. $\mathbf{v}_{\mathrm{S}}$ is the $N \times 1$ dimensional steering vector of the GNSS signal and it can be calculated as follows [21]:

$$\mathbf{v}_{\mathrm{s}} = \left(\mathrm{e}^{\mathrm{j}\frac{2\pi}{\lambda}\mathbf{P}_1^{\mathrm{T}}\mathbf{I}(\xi,\zeta)}, \mathrm{e}^{\mathrm{j}\frac{2\pi}{\lambda}\mathbf{P}_2^{\mathrm{T}}\mathbf{I}(\xi,\zeta)}, \ldots, \mathrm{e}^{\mathrm{j}\frac{2\pi}{\lambda}\mathbf{P}_N^{\mathrm{T}}\mathbf{I}(\xi,\zeta)}\right)^{\mathrm{T}} \tag{34}$$

where $\mathbf{P}_n$ is the coordinate of the n-th antenna element, λ is the wavelength of the GNSS signal, $\mathbf{I}(\xi,\zeta)$ is the unit directional vector of the GNSS signal and it can be calculated as follows:

$$\mathbf{I}(\xi,\zeta) = \begin{bmatrix} \cos(\xi)\cos(\zeta) & \cos(\xi)\sin(\zeta) & \sin(\xi) \end{bmatrix} \tag{35}$$

where ξ, ζ are elevation angle and azimuth angle of the GNSS signal, respectively. Antenna array weight vector $\mathbf{w}$ can be calculated as follows [22], [23]:

$$\mathbf{w} = \left(\mathbf{b}^{\mathrm{H}}\mathbf{R}_{xx}^{-1}\mathbf{b}\right)^{-1}\mathbf{R}_{xx}^{-1}\mathbf{b} \tag{36}$$

where $\mathbf{R}_{xx}$ is the $N \times N$ dimensional auto-correlation matrix of the received signal (including GNSS signal, jamming signal and noise), $\mathbf{b}$ is the $N \times 1$ dimensional constraint vector. Space-domain anti-jamming channel can be implemented by two algorithms, i.e. minimum variance distortion-less response (MVDR) algorithm [22] and power inversion (PI) algorithm [23]. For the MVDR algorithm, $\mathbf{b} = \mathbf{v}_{\mathrm{S}}$ [22]; for the PI algorithm, $\mathbf{b} = \mathbf{e}$, where $\mathbf{e}$ is a $N \times 1$ dimensional vector which is shown as follows [23]:

$$\mathbf{e} = \begin{pmatrix} 1 & 0 & \ldots & 0 \end{pmatrix}^{\mathrm{T}}. \tag{37}$$

Substituting $\mathbf{b}$ into (36), and then substituting formula (36) into (33), we can get the channel frequency-domain functions of the MVDR algorithm and the PI algorithm which are shown in the following formula (38) and (39), respectively.

$$H_{\mathrm{MVDR}}(f) = 1, \tag{38}$$

$$H_{\mathrm{PI}}(f) = \left(\left(\mathbf{e}^{\mathrm{H}}\mathbf{R}_{xx}^{-1}\mathbf{e}\right)^{-1}\mathbf{R}_{xx}^{-1}\mathbf{e}\right)^{\mathrm{H}}\mathbf{v}_{\mathrm{s}}. \tag{39}$$

Substituting formula (38) and formula (39) into (17), respectively, we can find $Q(f)$ are even functions in these two cases. That means condition 1 holds true. As a result, space-domain anti-jamming channels implemented by the MVDR algorithm and the PI algorithm will not introduce pseudo-code measurement bias.

4. Simulation Results

4.1 Overview

In order to verify the correctness of the analysis model, three kinds of channels, i.e. sine type group delay channel, frequency-domain anti-jamming channel and space-domain anti-jamming channel, are simulated. BDS B3I signal is simulated as an example of the GNSS signal. Radio frequency, pseudo-code rate and signal length of the B3I signal are 1268.52 MHz, 10.23 MHz and 1 second, respectively. In practice, the carrier-to-noise ratios (C/N_0) of the GNSS signal varies from 40 dB·Hz to 50 dB·Hz. As a result, we design three C/N_0s, i.e. 40 dB·Hz, 45 dB·Hz and 50 dB·Hz, in the following simulations. Sample rate is 35 MHz. The interval of the early code and the late code is 1 chip. Simulation is based on Matlab platform. Figure 3 shows the simulation flow chart. As Figure 3 shows, GNSS signal and noise are simulated at first. For frequency-domain anti-jamming channel and space-domain anti-jamming channel, jamming signals (dotted line) are also simulated. Then, they pass through channel. Next, signal after passing through channel is processed by software receiver. At last, we examine whether the correlation function is symmetrical and whether the pseudo-code measurement bias is introduced.

4.2 Sine Type Group Delay Channel

Five scenarios with different amplitude coefficients α, frequency coefficients β and GNSS signal C/N_0s are simulated. Scenario parameters are shown in Tab. 2.

Figure 4 and 5 show the results of the sine type group delay channel. Red, blue, green, pink and yellow are the results of the scenario 1 to 5, respectively. Figure 4 shows the correlation functions at $t = 0.9$ seconds. As Figure 4 shows, correlation functions in these five scenarios are basically symmetrical. Figure 5 shows pseudo-code measurement biases during the whole time span. As Figure 5 shows, pseudo-code measurement biases are around zero in different scenarios. Results verify that sine type group delay channel does not introduce pseudo-code measurement bias, which is consistent to the theoretical analysis.

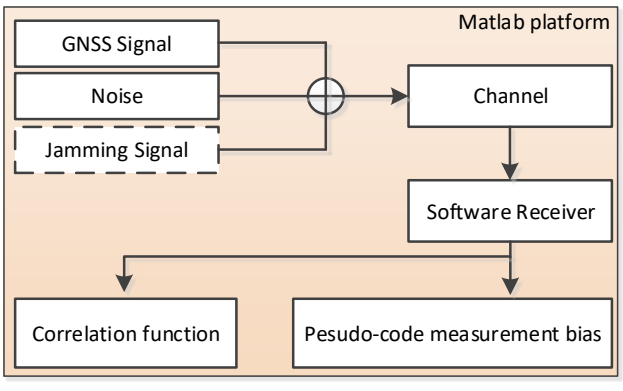

Fig. 3. Simulation flow chart.

Scenario	α	β	C/N_0
1	10 ns	10.23 MHz	50 dB·Hz
2	20 ns	10.23 MHz	50 dB·Hz
3	50 ns	10.23 MHz	45 dB·Hz
4	50 ns	5.115 MHz	45 dB·Hz
5	50 ns	1.023 MHz	40 dB·Hz

Tab. 2. Scenario parameters for the sine type group delay channels.

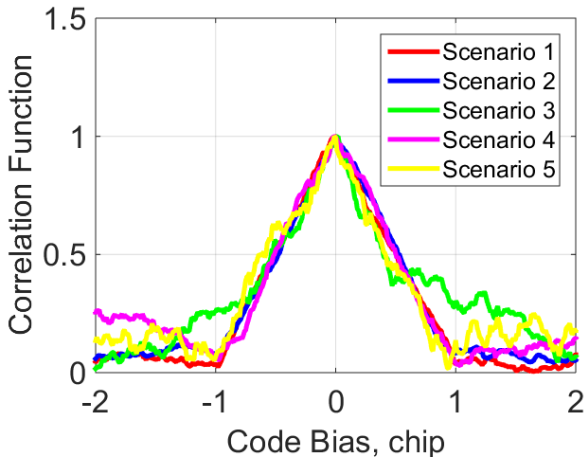

Fig. 4. Correlation functions at $t = 0.9$ seconds after GNSS signals pass through sine type group delay channels.

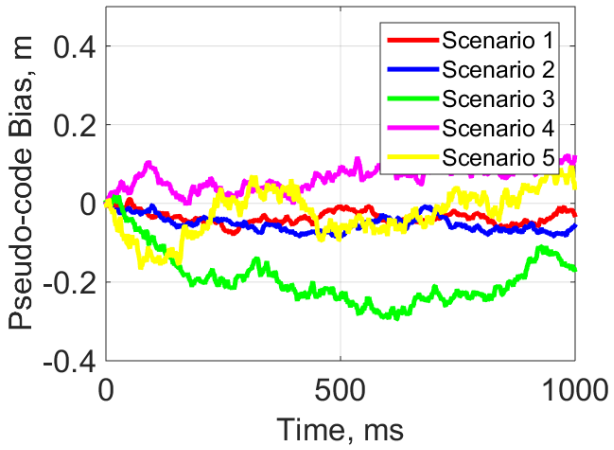

Fig. 5. Pseudo-code measurement biases during the whole time span after GNSS signals pass through sine type group delay channels.

4.3 Frequency-Domain Anti-Jamming Channel

Five scenarios with different offsets of the jamming center frequency relative to the GNSS signal frequency f_J, jamming bandwidths f_B, jamming signal group delays t_0 and GNSS signal C/N_0s are simulated. Scenario parameters are shown in Tab. 3.

Figure 6 and 7 show the results of the frequency-domain anti-jamming channel. Red, blue, green, pink and yellow are the results of the scenario 1 to 5, respectively.

Figure 6 shows the correlation functions at t = 0.9 seconds. As Figure 6 shows, correlation functions in these five scenarios are basically symmetrical. Figure 7 shows pseudo-code measurement biases during the whole time span. As Figure 7 shows, pseudo-code measurement biases are around zero in different scenarios. Results verify that frequency-domain anti-jamming channel does not introduce pseudo-code measurement bias, which is consistent to the theoretical analysis.

Scenario	f_J	f_B	t_0	C/N₀
1	2 MHz	0.5 MHz	0 ns	50 dB·Hz
2	2 MHz	1 MHz	5 ns	50 dB·Hz
3	2 MHz	2 MHz	10 ns	45 dB·Hz
4	3 MHz	2 MHz	20 ns	45 dB·Hz
5	4 MHz	2 MHz	30 ns	40 dB·Hz

Tab. 3. Scenario parameters for the frequency-domain anti-jamming channels.

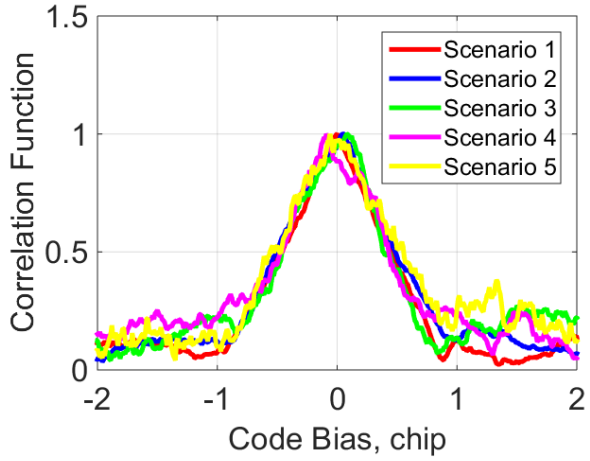

Fig. 6. Correlation functions at t = 0.9 seconds after GNSS signals pass through frequency-domain anti-jamming channels.

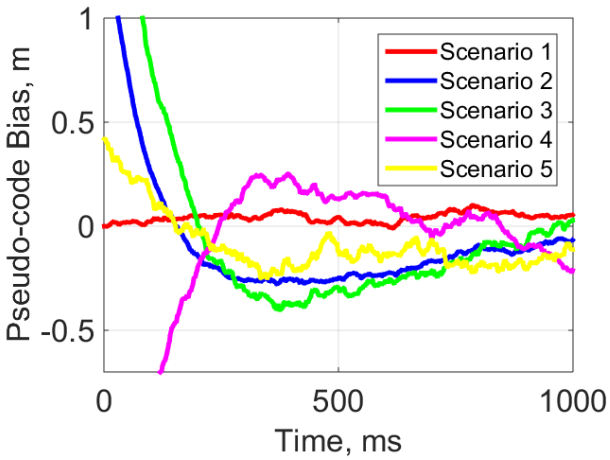

Fig. 7. Pseudo-code measurement biases during the whole time span after GNSS signals pass through frequency-domain anti-jamming channels.

4.4 Space-Domain Anti-Jamming Channel

An antenna array with seven antenna elements is simulated. Five scenarios with different numbers of jamming signals, different types of jamming signals (including continuous-wave (CW) jamming signal and wideband jamming signal), different elevation angles (degree) and azimuth angles (degree) of jamming signals and GNSS signals, different GNSS signal C/N_0s are simulated. The jamming-signal-rates (JSRs) of these jamming signals are 70 dB. Scenario parameters are shown in Tab. 4.

Figure 8 and 9 show the results of the space-domain anti-jamming channel implemented by the PI algorithm. Red, blue, green, pink and yellow are the results of the scenario 1 to 5, respectively. Figure 8 shows the correlation functions at t = 0.9 seconds. As Figure 8 shows, correlation functions in these five scenarios are basically symmetrical. Figure 9 shows pseudo-code measurement biases during the whole time span. As Figure 9 shows, pseudo-code measurement biases are around zero in different scenarios.

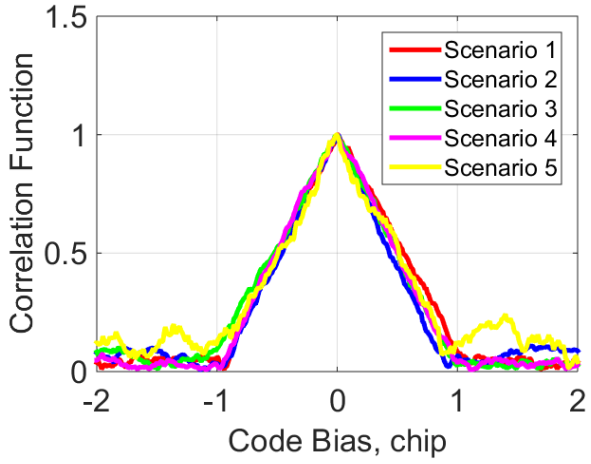

Fig. 8. Correlation functions at t = 0.9 seconds after GNSS signals pass through space-domain anti-jamming channels implemented by the PI algorithm.

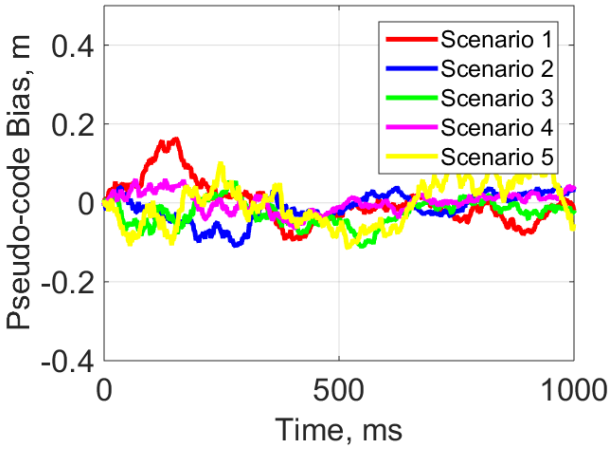

Fig. 9. Pseudo-code measurement biases during the whole time span after GNSS signals pass through space-domain anti-jamming channels implemented by the PI algorithm.

Results verify that space-domain anti-jamming channel implemented by the PI algorithm does not introduce pseudo-code measurement bias, which is consistent to the theoretical analysis.

Figure 10 and 11 show the results of the space-domain anti-jamming channel implemented by the MVDR algorithm. Red, blue, green, pink and yellow are the results of the scenario 1 to 5, respectively. Figure 10 shows the correlation functions at $t = 0.9$ seconds. As Figure 10 shows, correlation functions in these five scenarios are basically symmetrical. Figure 11 shows pseudo-code measurement biases during the whole time span. As Figure 11 shows, pseudo-code measurement biases are around zero in different scenarios. Results verify that space-domain anti-jamming channel implemented by the MVDR algorithm does not introduce pseudo-code measurement bias, which is consistent to the theoretical analysis.

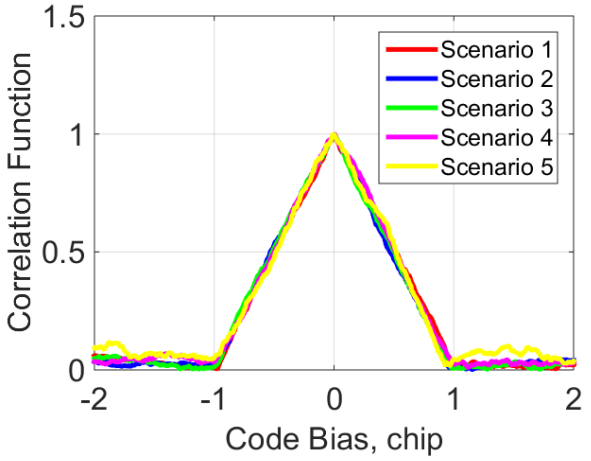

Fig. 10. Correlation functions at $t = 0.9$ seconds after GNSS signals pass through space-domain anti-jamming channels implemented by the MVDR algorithm.

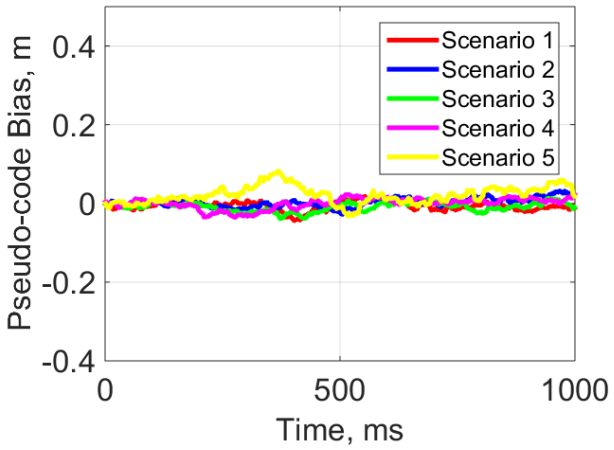

Fig. 11. Pseudo-code measurement biases during the whole time span after GNSS signals pass through space-domain anti-jamming channels implemented by the MVDR algorithm.

Scenario	Signal types	Start & end time	Elevation angle	Azimuth angle	C/N₀
1	GNSS signal	0 – 1 s	30°	280°	50 dB·Hz
	CW interference	0.4 – 1 s	15°	200°	-
	Wideband interference	0.4 – 1 s	5°	100°	-
2	GNSS signal	0 – 1 s	50°	130°	50 dB·Hz
	CW interference	0.4 – 1 s	10°	50°	-
	Wideband interference 1	0.4 – 1 s	5°	200°	-
	Wideband interference 2	0.4 – 1 s	5°	270°	-
3	GNSS signal	0 – 1 s	60°	90°	45 dB·Hz
	Wideband interference 1	0.4 – 1 s	5°	10°	-
	Wideband interference 2	0.4 – 1 s	10°	150°	-
	Wideband interference 3	0.4 – 1 s	15°	300°	-
4	GNSS signal	0 – 1 s	75°	120°	45 dB·Hz
	CW interference 1	0.4 – 1 s	10°	50°	-
	CW interference 2	0.4 – 1 s	10°	200°	-
	CW interference 3	0.4 – 1 s	10°	330°	-
5	GNSS signal	0 – 1 s	65°	110°	40 dB·Hz
	CW interference 1	0.4 – 1 s	10°	70°	-
	CW interference 2	0.4 – 1 s	10°	190°	-
	Wideband interference 2	0.4 – 1 s	10°	350°	-

Tab. 4. Scenario parameters for the space-domain anti-jamming channels.

5. Conclusions

This paper studies the influence of channel's non-ideal characteristic on pseudo-code measurement bias in depth. Analysis model is constructed at first and based on the general analysis, four sufficient conditions of channel characteristic for unbiased pseudo-code measurement are proposed. Analysis model is applied to three typical channels, i.e. sine type group delay channel, frequency-domain anti-jamming channel and space-domain anti-jamming channel, and we theoretically analyzed that these channels would not introduce pseudo-code measurement biases. Simulation results are consistent with theoretical analysis so that the theoretical analysis' correctness is verified.

Acknowledgments

Research was supported by Beijing Institute of Tracking and Telecommunication Technology.

References

[1] KAPLAN, E. D., HEGARTY, C. J. *Understanding GPS/GNSS: Principles and Applications*. 3rd ed. Artech House, 2017. ISBN: 1630810580

[2] WANG, Y. D., YE, X. Z., CHEN, S., et al. Study on the influence of space-time adaptive processor on single point position and real-time kinematic for GNSS antenna array anti-jamming receiver. *IET Radar, Sonar & Navigation*, 2025, vol. 19, no. 1, p. 1–11. DOI: 10.1049/rsn2.70035

[3] TAN, X. R., XU, J. N., LI, F. N., et al. A new GM(1,1) model suitable for short-term prediction of satellite clock bias. *IET Radar, Sonar & Navigation*, 2022, vol. 16, no. 12, p. 2040–2052. DOI: 10.1049/rsn2.12315

[4] YU, C., LI, Z. L., PENNA, N. T. Interferometric synthetic aperture radar atmospheric correction using a GPS_based iterative tropospheric decomposition model. *Remote Sensing of Environment*, 2018, vol. 204, p. 109–121. DOI: 10.1016/j.rse.2017.10.038

[5] KLOBUCHAR, J. A. Ionospheric time-delay algorithm for single-frequency GPS users. *IEEE Transactions on Aerospace and Electronic Systems*, 1987, vol. AES-23, no. 3, p. 325–331. DOI: 10.1109/TAES.1987.310829

[6] VAN DIERENDONCK, A. J., FENTON, P., FORD, T. Theory and performance of narrow correlator spacing in a GPS receiver. *Navigation*, 1993, vol. 39, no. 3, p. 265–283. DOI: 10.1002/j.2161-4296.1992.tb02276.x

[7] BHUIYAN, M. Z. H., ZHANG, J., LOHAN, E. S., et al. Analysis of multipath mitigation techniques with land mobile satellite channel model. *Radioengineering*, 2012, vol. 21, no. 4, p. 1067–1077. ISSN: 1210-2512

[8] CHEN, F. Q., NIE, J. W., LI, B. Y., et al. Distortionless space-time adaptive processor for global navigation satellite system receiver. *Electronic Letters*, 2015, vol. 51, no. 25, p. 2138–2139. DOI: 10.1049/el.2015.2832

[9] DAI, X. Z., NIE, J. W., CHEN, F. Q., et al. Distortionless space-time adaptive processor based on MVDR beamformer for GNSS receiver. *IET Radar, Sonar & Navigation*, 2017, vol. 11, no. 10, p. 1488–1494. DOI: 10.1049/iet-rsn.2017.0168

[10] WANG, Y. D., LIU, W. X., HUANG, L., et al. Distortionless pseudo-code tracking space-time adaptive processor based on the PI criterion for GNSS receiver. *IET Radar, Sonar & Navigation*, 2020, vol. 14, no. 12, p. 1984–1990. DOI: 10.1049/iet-rsn.2020.0189

[11] ZHU, X. W., LI, Y. L., YONG, S. W. A novel definition and measurement method of group delay and its application. *IEEE Transactions on Instrumentation and Measurement*, 2009, vol. 58, no. 1, p. 229–233. DOI: 10.1109/TIM.2008.927197

[12] XIAO, Z. B., HUANG, Y. B., TANG, X. M., et al. Fourier decomposition model of group delay and its estimation method (in Chinese). *Journal of National University of Defense Technology*, 2021, vol. 43, no. 5, p. 72–79. DOI: 10.11887/j.cn.202105008

[13] LIU, Y. Q., CHEN, L., YANG, Y., et al. Theoretical evaluation of group delay on pseudorange bias. *GPS Solutions*, 2019, vol. 23, no. 3, p. 1–12. DOI: 10.1007/s10291-019-0861-z

[14] ZHOU, H. W., WEI, J. L., ZHANG, X. Q., et al. Research on non-ideal property of payload core device on navigation satellite (in Chinese). *Journal of Huazhong University of Science & Technology (Natural Science Edition)*, 2014, vol. 42, no. 7, p. 118–123.

[15] BETZ, J. W. Effect of linear time-invariant distortions on RNSS code tracking accuracy. In *Proceedings of the 15th International Technical Meeting of the Satellite Division of the Institute of Navigation (ION GPS 2002)*. Portland (Oregon, USA), 2002, p. 1636–1647.

[16] SOELLNER, M., KOHL, R., LUETKE, W., et al. The impact of linear and non-linear signal distortions on Galileo code tracking accuracy. In *Proceedings of the 15th International Technical Meeting of the Satellite Division of the Institute of Navigation (ION GPS 2002)*, Portland (Oregon, USA), 2002, p. 1270–1285.

[17] HAUSCHILD, A., MONTENBRUCK, O. A study on the dependency of GNSS pseudorange biases on correlator spacing. *GPS Solutions*, 2016, vol. 20, no. 2, p. 159–171. DOI: 10.1007/s10291-014-0426-0

[18] HAUSCHILD, A., MONTENBRUCK, O. The effect of correlator and front-end design on GNSS pseudorange biases for geodetic receivers. *Navigation*, 2016, vol. 63, no. 4, p. 443–453. DOI: 10.1002/navi.165

[19] MULLER, T. Performance degradation in GPS-receivers caused by group delay variations of SAW-filters. In *1998 IEEE MTT-S International Microwave Symposium Digest*. Baltimore (MD, USA), 1998, vol. 2, p. 495–498.

[20] ZHANG, T. Q., ZHANG, X. M., LU, M. Q. Effect of frequency domain anti-jamming filter on satellite navigation signal tracking performance. In *China Satellite Navigation Conference 2013*. Wuhan (China), 2013, p. 507–516. DOI: 10.1007/978-3-642-37398-5_46

[21] VAN VEEN, B. D., BUCKLE, K. M. Beamforming: A versatile approach to spatial filtering. *IEEE ASSP Magazine*, 1988, vol. 5, no. 2, p. 4–24. DOI: 10.1109/53.665

[22] FU, Z., HOMBOSTEL, A., HAMMESFAHR, J., et al. Suppression of multipath and jamming signals by digital beamforming for GPS/Galileo applications. *GPS Solutions*, 2003, vol. 6, no. 4, p. 257–264. DOI: 10.1007/s10291-002-0042-2

[23] COMPTON, R. T. The power-inversion adaptive array: Concept and performance. *IEEE Transactions on Aerospace and Electronic Systems*, 1979, vol. AES-15, no. 6, p. 803–814. DOI: 10.1109/TAES.1979.308765

About the Authors ...

Yaoding WANG (corresponding author) was born in 1992. He received his M.S. and Ph.D. degrees from the National University of Defense Technology, Changsha, China in 2016 and 2020, respectively. He is currently working in Beijing Institute of Tracking and Telecommunication Technology. His research interests include GNSS data processing.

Xiang FANG was born in 1986. He received his M.S. degree from Tsinghua University, Beijing, China in 2012. He is currently working in Beijing Institute of Tracking and Telecommunication Technology. His research interests include space system.

Mimi LU was born in 1991. She received her M.S. degree from Beijing Foreign Studies University, Beijing, China in 2017. She is currently working in Beijing Institute of Tracking and Telecommunication Technology. Her research interests include space system.